Ionic conductivity and heat capacity of the solid electrolytes $M\mathrm{Ag_4I_5}$ near T_c*

R. A. Vargas, M. B. Salamon, and C. P. Flynn
Department of Physics and Materials Research Laboratory, University of Illinois, Urbana, Illinois 61801
(Received 8 August 1977)

We have measured the conductivities σ and heat capacities C_p of $M\mathrm{Ag_4I_5}$-family solid electrolytes through the temperature range centered near 200 K, of their order-disorder transformations. Here, M represents Rb, K, and $\mathrm{NH_4}$. The experiments were performed on pure single-crystal specimens. The heat capacities of all the samples yielded approximately the same critical exponent, $\alpha = 0.15$, both above and below T_c. This value is close to that predicted by the Ising model. C_p and σ were measured simultaneously by the ac method. We find for each salt that $d(\ln\sigma)/dT$ is accurately proportional to C_p. This result is also derived theoretically by a calculation which takes full account of the way short-range order determines both C_p and σ. The observations cannot be reproduced by mean-field theories. By fitting the experimental data to theory we find that the saddle points through which diffusion occurs are insensitive to short-range order. The heat-capacity results are compatible with a conclusion that approximately 40 of the 56 Ag ions per unit cell are involved in the order-disorder transformation.

I. INTRODUCTION

A number of ionic solids have highly conducting phases far below their melting temperatures, with conductivities comparable to those of liquid electrolytes.[1] Sometimes termed "superionic" conductors,[2] these materials are of considerable technological interest as electrolytes for solid-state batteries. Many exhibit phase transitions into phases of lower conductivity. Some of these are second-order transitions, characterized by gradual changes in the conductivity and lambda anomalies in the specific heat.[3–5] Because of the wealth of information at hand concerning the detailed behavior of materials undergoing second-order transitions, these critical points may be used to investigate the materials and to study the relationship between ionic conductivity and the ordering of the mobile-ion species.

A prototypical system is the series of silver-ion conductors $M\mathrm{Ag_4I_5}$, where M may be Rb, K, or $\mathrm{NH_4}$. The second-order phase transitions occuring near 200 K have been partially characterized.[1] X-ray data have shown that the $\mathrm{RbAg_4I_5}$ transition involves a structural change from cubic to rhombohedral.[6] Specific-heat measurements have been used to demonstrate that the second-order transition is Ising-like; birefringence data show that it is similar to a cooperative Jahn-Teller transition.[5] Salamon has presented a model for the transition at 208 K in $\mathrm{RbAg_4I_5}$ which involves distortions of the iodine lattice to couple the ordering of the Ag ions at specific sites.[7] The first-order transition which occurs in these materials near 125 K will not be discussed here.

In this paper we extend the specific-heat and conductivity measurements on $\mathrm{RbAg_4I_5}$ to the remaining members of this class of compounds. In an earlier report we show that the ionic conductivity of $\mathrm{RbAg_4I_5}$ decreases smoothly near T_c and shows precursive behavior.[8] This is contrary to previous predictions[9] from mean-field models, which indicate that the ionic conductivity decreases as $(T - T_c)^{1/2}$ below T_c and is insensitive to order above T_c. In this paper we present a theory which goes beyond the mean-field approximation to predict that the activation energy for ionic conductivity should follow the ordering enthalpy of the system[8]; both effects are sensitive mainly to the short-range order surrounding each mobile ion. It will be shown that this prediction is borne out for all members of the family of ionic conductors examined in this work.

In Sec. II we present details of the experimental measurements by means of which we obtain simultaneous determinations of the specific heat and the temperature derivative of the resistivity for single-crystal samples. The results for the three salts, $\mathrm{RbAg_4I_5}$, $\mathrm{KAg_4I_5}$, and $\mathrm{NH_4Ag_4I_5}$ are presented in Sec. III. Section IV contains a theoretical discussion of the ionic conductivity near ordering transitions, with particular application to ionic conductors. A comparison of theory and experiment is made in Sec. V.

II. EXPERIMENTAL METHODS

When a sample absorbs heat periodically at a given temperature, the amplitude of the induced temperature oscillation is related to its specific heat.[10] Under desirable conditions for ac calorimeters, the temperature oscillation is so slow (compared to significant thermal-relaxation times of the sample), and its amplitude so small, that the system is at all times very close to equilibrium. For a thickness d, density ρ_s, and heat capacity C_s, the magnitude of the ac component of the sample temperature is approximately[10]

$$|\Delta T_s^{\rm ac}| = P_1/\omega_0(C_s\rho_s d) \ , \tag{1}$$

when the power input is

$$P(t) = P_0 + P_1 \exp(i\omega_0 t) + \cdots .$$

By this method, the specific heat can be measured as a function of some externally varied parameter, which, in our case, is the bath temperature. The ac technique provides a continuous record of the specific heat and gives high resolution provided that the amplitude of the temperature oscillation is small.

The ac modulation of sample temperature introduces modulations of other sample properties.[11] We shall be concerned with the relationship between the voltage V and the current I. I and V are linearly related by

$$V = R(T)I \ , \tag{2}$$

with the response function $R(T)$ temperature dependent. Then, for constant I and T_0,

$$V = I\left[R(T_0) + \left(\frac{dR}{dT}\right)_{T_0}\Delta T \exp(i\omega_0 t) + \cdots\right] . \tag{3}$$

By detecting the component of V at the fundamental frequency of temperature oscillation ω_0, we can therefore measure $(dR/dT)_{T_0}$.

In the present investigation, a sinusoidal ac current (frequency $\omega_1 >> \omega_0$) with constant amplitude I_1 was passed through the sample, and the amplitude V_1 of the voltage at frequency ω_0 detected by first filtering and demodulating the ac voltage signals. The narrow-band detection of a lock-in amplifier with reference frequency ω_0 was then employed to obtain the temperature derivative of the sample resistance $(dR/dT)_{T_0}$. This was measured as a function of the dc temperature T_0 of the system, while the sample specific heat, according to Eq. (1), was obtained simultaneously from the value of ΔT.

Single crystals of $M\mathrm{Ag_4I_5}$ (M = Rb, $\mathrm{NH_4}$, K) were grown in our laboratories using the solution technique[12] making use of MI and AgI reagents of 99.9% purity. Aqueous 0.57% molar hydroiodic acid HI was used as the solvent. The different steps necessary to prepare single crystals are explained in Ref. 12. An important point is that crystals of the form $M\mathrm{Ag_4I_5}$ could only be grown in a dry atmosphere (relative humidity less than 10%) and with adequate ventilation for at least the first 3 days of evaporation. Optically clear, octahedral crystals were produced in various sizes from 0.6 to 1.2 cm in diameter. Small single crystals were chosen as representative specimens for x-ray crystallographic identification. Buerger precession patterns showed quite uniform alignment and a cubic unit cell with a lattice constant of 11.24, 11.19, and 11.13 Å for M = Rb, $\mathrm{NH_4}$, and K, respectively. These values are in good agreement with previous determinations.[6] Chemical analyses of $\mathrm{RbAg_4I_5}$ yielded Ag-Rb atomic ratios of 4.2 ± 0.2.

The compounds $M\mathrm{Ag_4I_5}$ are thermodynamically unstable below 27, 32, and 36 °C for M = Rb, $\mathrm{NH_4}$, and K, respectively. At higher temperatures they undergo disproportionation reactions to form $M_2\mathrm{AgI_3}$ and AgI.[12] However, the rate of decomposition is extremely small in the absence of moisture. All steps in sample preparation were, for this reason, performed in a glove box filled with dry $\mathrm{N_2}$.

To produce specimens, the crystals were first cut with a diamond-impregnated wire into wafers of cross section ranging in area from 8 to 10 $\mathrm{mm^2}$. The opposite surfaces of the slices were ground parallel with each other and then polished to a thickness of approximately 0.1 mm using dry abrasives. The resulting slab-shaped samples are very brittle and must be handled with great care at all times.

Special efforts are required to make good electrical contact to the $M\mathrm{Ag_4I_5}$ (M = Rb, $\mathrm{NH_4}$, K) samples. It has been found that the most common interfaces, such as "parent-metal" electrodes, cause impedance-related problems which are particularly pronounced at high current densities. In previous dc-conductivity measurements made on polycrystalline specimens of $\mathrm{RbAg_4I_5}$ pressed into pellets, these contact problems were reduced by spring loading the samples between silver or amalgamated silver-foil electrodes, or by using mixtures of fine grains of $\mathrm{RbAg_4I_5}$ and Ag as the electrode materials.[13] However, uncertain grain boundary errors from contact resistance are always present in low-frequency ionic conductivity measurements on pressed-powder pellet samples. Similar contact problems were observed during the present investigation of $M\mathrm{Ag_4I_5}$ single crystals (M = Rb, $\mathrm{NH_4}$, K) when these less-satisfactory interfaces were used.

The contact problems were greatly reduced when diffused silver contacts were used as electrodes. We used 50-μm silver wires, coated with Ag paint dissolved in toluene; they were electrically heated while in contact with the sample over an area covered with silver powder. With these electrodes, no change in the sample impedance at constant temperature for frequencies higher than 500 Hz and current densities lower than 1 $\mathrm{mA/mm^2}$ could be observed over the course of several hours. All the measurements re-

ported here were made using this type of electrode interface.[14]

After the deposition of the four electrodes and the connection of the corresponding electrical leads to one face of a slab-shaped sample, two 25-μm type-K thermocouples were attached to the same face to monitor the average dc temperature of the sample and its induced temperature oscillations. Figure 1 shows the (S_1,S_2) thermocouple, for monitoring ΔT, flattened at the junction for better thermal contact, and attached to the sample by minute amounts of Dow-Corning silicone grease. The thermocouple for monitoring the average temperature of the sample, labeled (A,C), was electrically isolated from the sample by a very thin film of Ge RTV-108 silicone rubber. The face of the thermocouple maintained thermal contact with the sample, but the dc coupling to the electronic measuring system was eliminated. The opposite face of the sample was coated with colloidal graphite to maximize the absorption of optical heating pulses. Auxilliary measurements in the range $1.5 < \omega_0 < 10$ Hz confirmed that ΔT was inversely proportional to ω_0 in accordance with Eq. (1). The optimum operational chopping frequency was approximately 1.6 Hz.

The experimental arrangement used to measure ΔT and dR/dT simultaneously on one $M\mathrm{Ag_4I_5}$ crystal is a modification of the Simons apparatus.[11] The constant

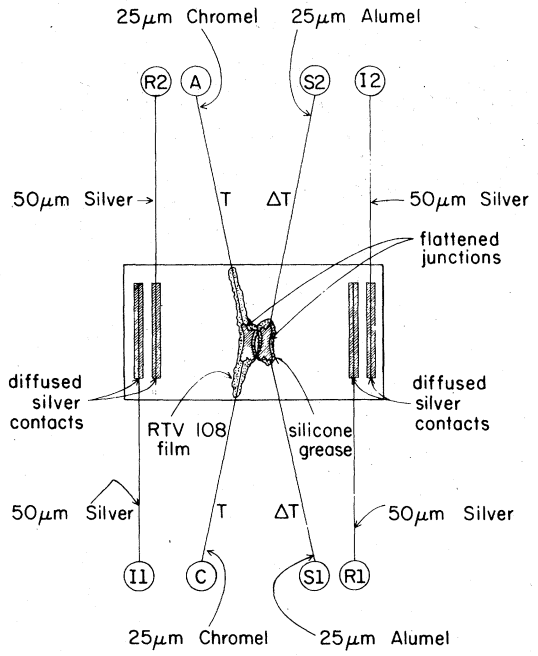

FIG. 1. Schematic diagram of sample. The current leads are labeled I_1 and I_2; the voltage leads, R_1 and R_2. S_1 and S_2 are the ac thermocouple leads; A and C extend to an external ice bath to permit measurement of the dc sample temperature.

ac current was produced by connecting a 100-kΩ standard resistance in series with the sample in the secondary of an isolation transformer whose primary was driven by a high-purity constant-amplitude sine-wave generator. The frequency of this signal was $\omega_1 = 10$ kHz and the current density about 0.1 mA/mm^2. The resulting ac voltage signals across the sample, modulated by the induced temperature oscillations at frequency $\omega_0 = 1.6$ Hz, were fed into a low-noise battery-operated preamplifier to eliminate pickup problems and to drive the demodulator. A low-pass filter at the demodulator output was used to attenuate higher-frequency components ($>\omega_0$) of the signal, in order both to reduce noise and to prevent overloading of the detection system. The filtered output went into the input of the preamp stage of a lock-in amplifier. The outputs of the two lock-in amplifiers giving ΔT and $I_0(dR/dT)\Delta T$ were recorded continuously as the average temperature of the sample was swept slowly through the phase transition.

The ac method does not give the absolute value of the specific heat when the heat flux to the sample is provided by means of mechanically chopped light. This problem is usually circumvented by normalizing the data to an absolute measurement at a specific temperature. Our results for the specific heat of $\mathrm{RbAg_4I_5}$ were normalized to the measurements of Wiedersich and Johnston[4] at a point near room temperature; the two measurements are then in agreement at lower temperatures. However, for $\mathrm{NH_4Ag_4I_5}$ and $\mathrm{KAg_4I_5}$ it was necessary to measure the absolute values of the specific heat. A quasiadiabatic pulse method was used. The resulting room-temperature values are as follows:

$\mathrm{RbAg_4I_5}$, $C_P = 68.3$ calories/(mole K);

$\mathrm{NH_4Ag_4I_5}$, $C_P = 80.6 \pm 2.4$ calories/(mole K);

$\mathrm{KAg_4I_5}$, $C_P = 72.8 \pm 2.2$ calories/(mole K).

III. RESULTS

A. $\mathrm{RbAg_4I_5}$

Preliminary reports of the experiments carried out on this compound have appeared elsewhere.[5,8] Figure 2 shows the sample resistance and Fig. 3 shows the logarithmic derivative of its conductivity $d(\ln\sigma)/dT$ near T_c. The latter exhibits critical behavior similar to that of the specific heat, which is also shown in Fig. 3. If the conductivity is assumed to take the Arrhenius form, the data of Fig. 2 yield the activation energy $U = 0.12$ eV for $213 < T < 300$ K and $U = 0.17$ eV for $180 < T < 205$ K. These values are in good agreement with previous determination from the dc conductivity.[13]

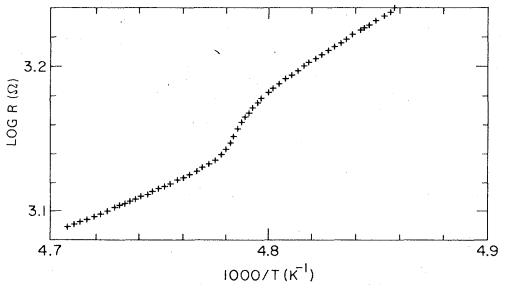

FIG. 2. Ionic resistance of $RbAg_4I_5$ as a fuanction of temperature through the disordering transformation.

Since C_P and $d(\ln\sigma)/dT$ were measured simultaneously in the vicinity of T_c we may examine their *relative* critical behavior without reference to fitting functions, exponents, or a choice of T_c. The experimental values of $d(\ln\sigma)/dT$ are plotted in Fig. 4 as a function of the molar specific heat C_P with the temperature as an implicit parameter. The curves cover three decades of reduced temperature above and below the peak. The solid line fitted to the data above and below T_c gives

$$\frac{d(\ln\sigma)}{dT} = \frac{\kappa}{RT_c}(C_P - B) \quad , \tag{4}$$

with $\kappa = 0.6105$ and $B = 24.09R$ for $RbAg_4I_5$. No attempt has been made to subtract the temperature-dependent portion of the lattice heat capacity, and this undoubtedly causes some deviations of the data points from linearity at small values of C_P far from the peak. We note that Eq. (4) holds accurately even where C_P is rounded.

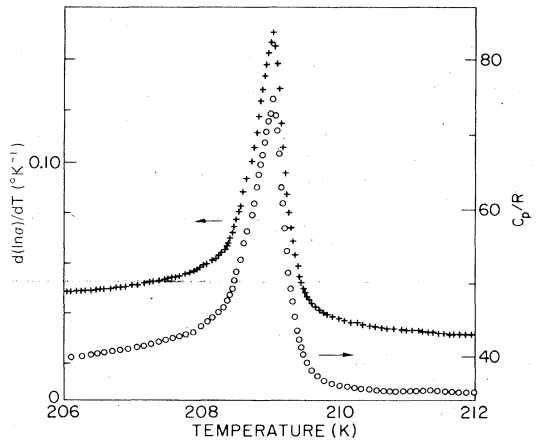

FIG. 3. Logarithmic temperature derivative of the ionic conductivity of $RbAg_4I_5$ as a function of temperature. The specific heat is shown for comparison.

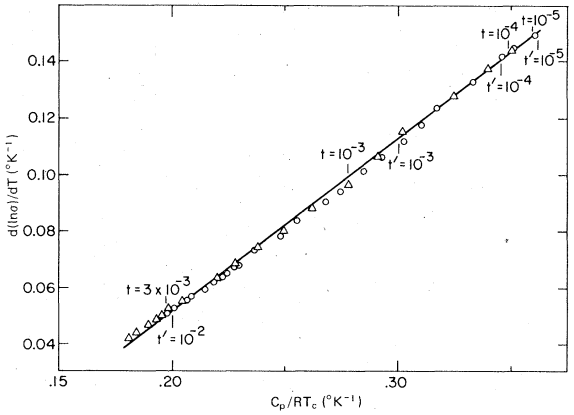

FIG. 4. Plot of $d\ln\sigma/dT$ against C_P with temperature as an implicit variable for $RbAg_4I_5$.

B. $NH_4Ag_4I_5$ and KAg_4I_5

The critical behavior of the specific heats of $NH_4Ag_4I_5$ and KAg_4I_5 near their second-order phase transitions were compared with the following power-law equations:

$$C_P^+(t) = (A^+/\alpha)(|t|^{-\alpha} - 1) + B^+, \quad T > T_c \quad , \tag{5a}$$

$$C_P^-(t) = (A^-/\alpha')(|t|^{-\alpha'} - 1) + B^-, \quad T < T_c \quad , \tag{5b}$$

where $t \equiv (T/T_c - 1)$ is the reduced temperature. Using a data-analysis technique developed by Lederman, Salamon, and Shacklette,[15] the specific heats C_P^+ and C_P^- were interpolated for equal values of $|t|$. By adjusting T_c, a linear relation was obtained between C_P^+ and C_P^- data points with the reduced temperature t as an implicit parameter. The intervals of reduced temperature above and below the peak fall in the range $10^{-4} \lesssim t \lesssim 10^{-1.5}$. Figures 5 and 6 show these results for $NH_4Ag_4I_5$ and KAg_4I_5, respectively. We conclude

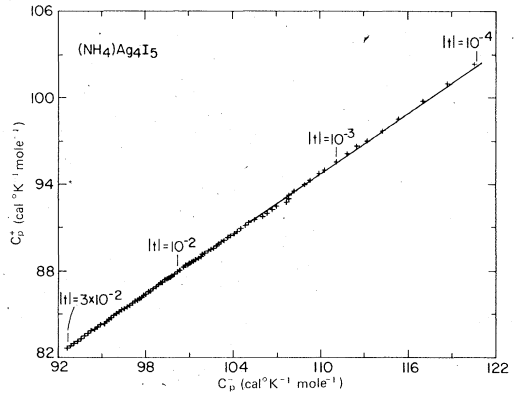

FIG. 5. Specific heat (C_P^+) above T_c vs the specific heat (C_P^-) below T_c. The data establish the scaling law for $NH_4Ag_4I_5$.

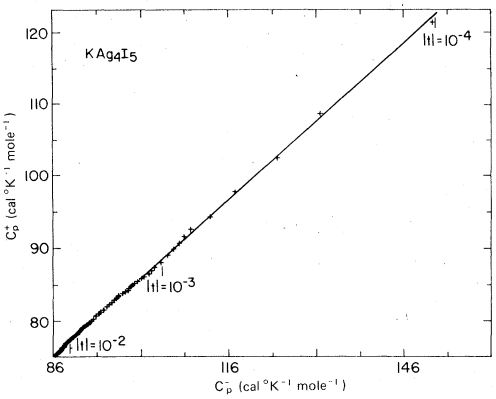

FIG. 6. Specific heat (C_P^+) above T_c vs the specific heat (C_P^-) below T_c. The data establish the scaling law for KAg_4I_5.

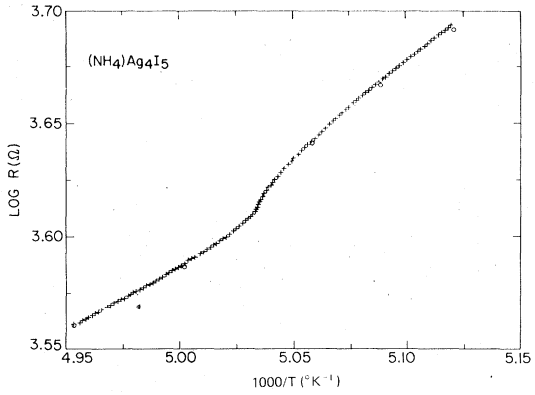

FIG. 7. Resistance of $NH_4Ag_4I_5$ sample. The points marked by symbols + and ○ are obtained by integration of the derivative signal and direct measurement, respectively.

that in these systems the scaling law $\alpha = \alpha'$ is verified just as for $RbAg_4I_5$.[5] The results are summarized in Table I. We note that $B^+ - A^+/\alpha$ equals $B^- - A^-/\alpha'$ within experimental uncertainty, so that correction terms appear unnecessary.

The conductivity results for $NH_4Ag_4I_5$ and KAg_4I_5 were analyzed by the procedure described above for $RbAg_4I_5$. Figure 7 shows the resistance $R(T)$ of $NH_4Ag_4I_5$ obtained by integrating the experimental values of dR/dT through the critical region. dc-resistance measurements at several temperatures in the same range are also indicated for comparison. The experimental values of $d(\ln\sigma)/dT$ are plotted in Fig. 8 as a function of the molar specific heat C_P with the temperature an implicit variable. The curves cover three decades of reduced temperature above and below the peak. The analogous experimental data for KAg_4I_5 are shown in Figs. 9 and 10, respectively. The results are compiled in Tables II and III. By way of summary, one may note that in all these materials there exists an accurate proportionality between C_P and $d(\ln\sigma)/dT$. The origins of this novel property comprise the principal subject matter of Sec. IV.

It is worth mentioning, finally, that specific-heat measurements at lower temperature on $NH_4Ag_4I_5$ and KAg_4I_5 reveal signs of a first-order phase transition similar to that of $RbAg_4I_5$ at 122 K. The transition temperatures are $T_c = 134.7$ K for $NH_4Ag_4I_5$ and $T_c = 138.6$ K for KAg_4I_5. Table IV shows how the transition temperature of the class-I and class-II phase transformations varies with cation species. These effects are in turn related to the size of the cubic unit cell in the high-temperature phases.

IV. THEORY OF CONDUCTIVITY

The most convenient description of diffusion process in the regime near the 200-K transitions is provided by classical statistical mechanics. Quantum phenomena cannot be important since the thermal wavelength $\lambda = h/(3k_B TM)^{1/2} \sim 2 \times 10^{-9}$ cm of Ag ions is very much less than the intersite spacing. In addition, the temperature is above or comparable with the Debye temperature, at which thermal properties

TABLE I. Values of the fitting parameters for the specific heat of the MAg_4I_5 compounds. Values for the parameters are in calories/mole K. "Range" refers to the values of $\log_{10}|1 - T/T_c|$.

Parameters	$RbAg_4I_5$	KAg_4I_5	$NH_4Ag_4I_5$	ϵ expansion	Series
Range					
$T < T_c$	−0.4 to −3.7	−1.5 to −3.7	−1.7 to −4.2		
$T > T_c$	−0.4 to −3.7	−1.8 to −3.5	−1.7 to −3.5		
A^+		1.90 ± 0.1	2.05 ± 0.05		
B^+	60.1 ± 0.2	53.2 ± 1.0	59.6 ± 0.5		
B^-	65.6 ± 0.2	54.0 ± 1.0	60.2 ± 0.5		
A^+/A^-	0.46 ± 0.01	0.69 ± 0.01	0.70 ± 0.01	0.53	0.62 ± 0.03
$\alpha = \alpha'$	0.145 ± 0.02	0.15 ± 0.01	0.15 ± 0.02	0.08	0.125
T_c	208.605 K	194.135 K	198.68 K		

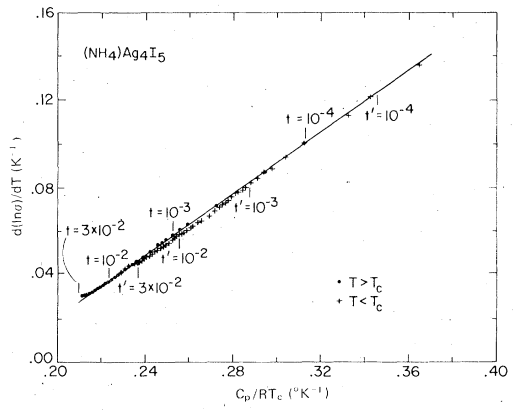

FIG. 8. Plot of $d(\ln\sigma)/dT$ against C_P for KAg_4I_5 with temperature an implicit variable. The straight line is a least-squares fit to the data.

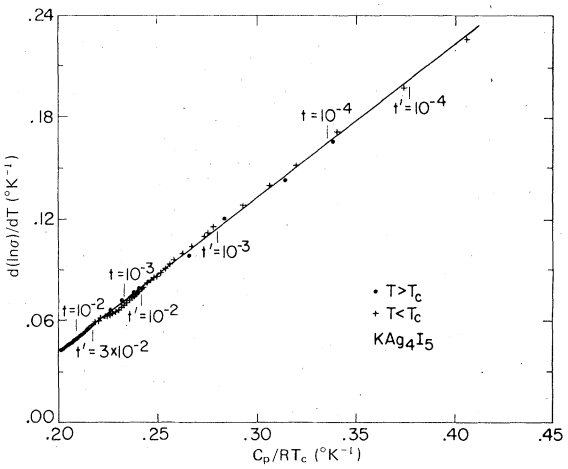

FIG. 10. Plot of $d(\ln\sigma)/dt$ against C_P for KAg_4I_5 with temperature an implicit variable. The straight line is a least-squares fit to the data.

approach classical values. A large body of evidence establishes that diffusion processes in crystals do not exhibit noticeable departures from their high-temperature behavior under these circumstances.[16]

At the same time, a description of diffusion in these disordered materials presents a many-body problem of considerable complexity, in that the jump rate is determined by the many-body potential energy of interaction among all the atoms. We shall call this potential energy $V(\vec{s})$, in which the mass weighted hypervector $\vec{s}$ locates the positions of all the atoms in the crystal. The systems of interest here contain a large number of interacting mobile particles. Rather than all jumps being equivalent, as for successive jumps of an isolated defect, the atomic displacements causing conduction in solid electrolytes occur in a wide variety of circumstances determined by the local order near the jump path. The approximate calculation that follows shows in fact that short-range order, manifested by correlations among the positions of the mobile atoms, is the dominant factor determining the defect mobility near the ordering transition. Hopping models[3,17] that require the diagonalization of a matrix of hopping rates, with or without polaron assumptions, are not well suited to this problem. Our calculations show, and the experiments confirm, that the required hopping rates are explicitly configuration dependent, through the influence of short-range order on the jump dynamics. An explicit treatment of the dynamics that enter into the diffusion jump is therefore necessary.

It is possible to approach this problem at a fundamental level using methods of classical statistical mechanics analogous to those employed by Slater[18] for molecules and Vineyard[19] for solids. The potential energy function $V(\vec{s})$, has minima in configuration space that correspond to stable configurations of the particles. Dynamical processes in which the representative point passes from the neighborhood of one minimum γ to a neighboring minimum γ' constitute the diffusion jumps of interest here. A boundary sur-

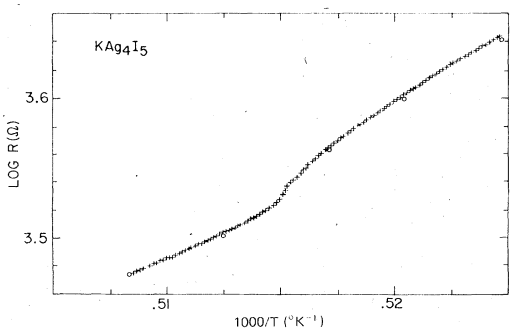

FIG. 9. Resistance of KHg_4I_5 sample. The points marked by symbols + and ○ are obtained by integration of derivative signal and direct measurement, respectively.

TABLE II. Activation energy of charge transport in MAg_4I_5 (M = Rb, NH_4, K) above and below the critical region of their corresponding class-II phase transitions.

Compound	Temperature range (K)	U (eV)
$RbAg_4I_5$	$213 < T < 300$	0.12
	$180 < T < 205$	0.17
$NH_4Ag_4I_5$	$202 < T < 300$	0.117
	$160 < T < 195$	0.162
KAg_4I_5	$196 < T < 300$	0.12
	$160 < T < 190.6$	0.18

TABLE III. Constant of proportionality between $d(\ln\sigma)dT$ and C_p for MAg_4I_5 (M = Rb, NH_4, K) in the critical region of their corresponding class-II transitions.

Compound	κ	Region of fit
$RbAg_4I_5$	0.6105	$-5.0 \leq \log_{10} t \leq -1.5$
$NH_4Ag_4I_5$	0.6825	$-4.5 \leq \log_{10} t \leq -1.7$
KAg_4I_5	0.8929	$-4.5 \leq \log_{10} t \leq -1.7$

face $\gamma\gamma'$ separating the two regions can be constructed on top of the potential ridge between the two minima. Configuration space is thus partitioned by a network of hypersurfaces into volumes associated with individual configurations. By definition, a jump is completed each time the representative point passes from γ through $\gamma\gamma'$ to γ'. The rate $w_{\gamma\gamma'}$ at which a particular jump occurs in thermal equilibrium is readily obtained as the number of representative points that cut through $\gamma\gamma'$ each second in an equilibrating ensemble. We shall return to the evaluation of the rate for the system of interest after a number of secondary but still important points are clarified.

One complication is that the jump rates $w_{\gamma\gamma'}$ thus calculated are not precisely the quantities needed to obtain the diffusion coefficient, because successive jumps of one mobile defect may not be mutually independent.[20] There is every reason to expect that this effect has negligible influence on the temperature dependence of diffusivity in the present application. If vacant interstitial sites were so rare that they limited the jump rate, then the most probable jump of a freshly displaced interstitial would be back to its former newly vacant site, thereby nullifying the first jump. For approximately tetrahedral coordination this *correlation effect* reduces the effective jump rate by a *correlation factor* of 0.50. But in the present application only $\frac{2}{7}$ of the interstitial sites are occupied, so the mean asymmetry of the vacant site distribution present immediately after a jump is reduced to about 29% of its value for the low-concentration limit. It follows that the correlation factor is increased to approximately 0.85 in the cases of interest here. The departure from unity is small, and possible temperature variations of this effect caused by its dependence on short-range order, neglected in this approximate discussion, are not of significant concern.

TABLE IV. Lattice constant of the cubic phase of the compounds MAg_4I_5 (M = Rb, NH_4, K), and transition temperature of their class-I and class-II phase transformations.

	a (Å)	$T_{c\mathrm{I}}$ (K)	$T_{c\mathrm{II}}$ (K)
$RbAg_4I_5$	11.24	122	208.6
$NH_4Ag_4I_5$	11.19	134.7	198.7
KAg_4I_5	11.13	138.6	194.1

Long-range order also offers potentially severe and complicated changes in the diffusion behavior. The main effect can be understood by comparison with the example of order-disorder transformations in binary alloys such as β-brass.[21] At low temperatures the two components, Cu and Zn, diffuse on independent sublattices with distinct defect populations, whereas above the order-disorder transformation they share all sites and defects. The effect of the transformation on the correlation factor connecting jump rates to diffusion coefficients is therefore significant. However, the effect is much less important in the present case because (a) the ordering only affects a fraction of the ions, (b) the ordering is only partial, and (c) there are so many empty sites that in any event the correlation factor remains close to unity as demonstrated above. The influence of long-range order will therefore be ignored completely in our final result. We shall see later that an accurate experimental check is available to confirm the validity of this approximation.

The final complication concerns the connection between the jump rate and conduction. We can obtain the conductivity from the jump rate using the Nernst-Einstein equation only for charge carriers that diffuse in the absence of perturbing local fields; interactions that modify the carrier density (as when carriers of opposite sign bind together) cause related changes in the conductivity. We are not aware of any treatment of these interactions for the specific case of solid electrolytes. In the Appendix we therefore present a perturbative discussion of the conductivity in the presence of solid-state interactions. This treatment shows that the Onsager theory[22] of interaction effects on the conductivity must be modified to take account of the overlapping Debye-Hückel screens of successive anions in solid electrolytes. The drag effect is greately reduced, and the residual contribution from screening is probably insensitive to both temperature and local order, so that its effect on critical properties can be neglected.

We now turn to an explicit calculation of the thermal mean jump rate. An expression for the rate $w_{\gamma\gamma'}$ at which transitions take place from volume γ to volume γ' of configuration space can be written directly in terms of the classical distribution function.[23] When evaluated in terms of the potential energy function $V(\vec{s})$ the answer is

$$w_{\gamma\gamma'} = \nu_{\gamma\gamma'} \exp[-(G_{\gamma\gamma'} - G_\gamma)/k_B T] \ , \tag{6}$$

in which

$$G_{\gamma\gamma'} = -k_B T \ln \int_{\gamma\gamma'} d^{3N-1}\vec{s}\, e^{-V(\vec{s})/k_B T} \ , \tag{7}$$

$$G_\gamma = -k_B T \ln \int_{\gamma} d^{3N}\vec{s}\, e^{-V(\vec{s})/k_B T} \ . \tag{8}$$

Here, for a crystal of N atoms, the integral giving $G_{\gamma\gamma'}$ extends over the $(3N-1)$-dimensional hypersurface separating γ from γ' and that giving G_γ extends over the $3N$-dimensional volume γ. The quantity $v_{\gamma\gamma'}$ is the perpendicular mean velocity with which representative points cut $(\gamma\gamma')$.

The total rate W at which diffusion jumps take place in a crystal in equilibrium can now be obtained as

$$W = \sum_{\gamma}' \sum_{\gamma'}' P_\gamma w_{\gamma\gamma'} \quad , \tag{9}$$

in which P_γ is the probability

$$P_\gamma = e^{-G_\gamma/k_BT} \Big/ \sum_{\gamma}' e^{-G_\gamma/k_BT} \quad , \tag{10}$$

with which configuration γ occurs. The summations extend over all distinguishable configurations γ and all distinguishable jump paths $\gamma\gamma'$. If the crystal of N atoms contains ηN mobile interstitials, the mean jump rate of each interstitial is

$$\langle w \rangle = \frac{W}{\eta N} = \sum_{\gamma'}' \sum_{\gamma} v_{\gamma\gamma'} \exp(-G_{\gamma\gamma'}/k_BT) \Big/ \eta N \sum_{\gamma}' \exp(-G_\gamma/k_BT) \quad , \tag{11}$$

from which the ionic diffusion coefficient and hence the mobility may be calculated by means of the simplifying assumptions discussed earlier.

Both the physical content and the complexity of the conductivity result are concealed in the summations of Eq. (11). To make contact with experimentally accessible quantities we must evaluate Eq. (11) in terms of the potential energy function $V(\vec{s})$. In particular, we wish to isolate the effect of interactions among interstitials on the conductivity by identifying that part of $V(\vec{s})$ caused by the interactions.

We write

$$V(\vec{s}) = V^0(\vec{s}) + V^i(\vec{s}) \quad , \tag{12}$$

with $V^i(\vec{s})$ representing the potential energy of interaction among the interstitials. To a major degree this division of V is arbitrary, since both V^0 and V^i are just $3N$-dimensional functions of the atomic positions. We take V^0 to give a virtual crystal model of the vibrational properties. It contains all dependence of the energy on interstitial location with respect to the embedding lattice and an average description of interactions among the interstitials. V^i then remains as a smooth function of $\vec{s}$ depending principally on the relative positions of the interstitials. A division of $V(\vec{s})$ in this way is always possible; we take the criteria for an optimal choice to be that V^0 conforms to the full crystal symmetry and that V^i be the smoothest possible function of atomic coordinates.

This division of V allows the many body problem to be simplified to manageable proportions. The virtual crystal portion, V^0, can be used to obtain jump rates for an idealized crystal lacking the complication of short range disorder, and the interaction part V^i then contains all effects of detailed short range order. For each jump geometry we can find virtual crystal values $G^0_{\gamma\gamma'}$ and G^0_γ of the functions $G_{\gamma\gamma'}$ and G_γ needed to predict the conductivity. The actual values in the presence of disorder then follow from a treatment of V^i.

In order to evaluate G^0_γ we diagonalize V about its minimum $V(\vec{s}^{\,\gamma})$ at $\vec{s}^{\,\gamma}$ in the volume γ:

$$V^0(\vec{s}-\vec{s}^{\,\gamma}) = V^0_\gamma + \sum_{\alpha=1}^{3N} \tfrac{1}{2}\omega^2_{\alpha\gamma} s^2_{\alpha\gamma} + \cdots \quad , \tag{13}$$

where the $s_{\alpha\gamma}$ are normal coordinates that diagonalize V and $\omega_{\alpha\gamma}$ are corresponding mode frequencies. Hence from Eq. (8) we find, neglecting terms of higher order than s^2:

$$G^0_\gamma = -kT \ln\left[e^{-V^0_\gamma/kT} \prod_{\alpha=2}^{3N} \left(\frac{2\pi k_BT}{\omega^2_\alpha} \right)^{1/2} \right] \quad . \tag{14}$$

To evaluate G_γ including $V^i(\vec{s})$ we assume that V^i is satisfactorily smooth near $\vec{s}^{\,\gamma}$ and expand it also in a Taylor series about $\vec{s}^{\,\gamma}$, now neglecting terms of s^2 and higher order. Then

$$\begin{aligned} V(\vec{s}-\vec{s}^{\,\gamma}) &= V^0_\gamma + \sum_\alpha \tfrac{1}{2}\omega^2_{\alpha\gamma} s^2_{\alpha\gamma} + \cdots \\ &\quad + V^i_\gamma + \sum_\alpha \lambda_\alpha s_{\alpha\gamma} + \cdots \\ &= V^0_\gamma + V^i_\gamma + \sum_\alpha \tfrac{1}{2}\omega^2_\alpha \left(s_{\alpha\gamma} + \frac{\lambda_\alpha}{\omega^2_\alpha} \right)^2 \\ &\quad - \sum \frac{\tfrac{1}{2}\lambda^2_\alpha}{\omega^2_\alpha} + \cdots \quad . \end{aligned} \tag{15}$$

By carrying out the integrals needed to obtain G_γ we now find, to the neglect of terms of second and higher powers in λ that

$$G_\gamma = G^0_\gamma + V^i_\gamma \quad , \tag{16}$$

with V^i_γ the values of $V^i(\vec{s})$ at the new minima $(s^\gamma_\alpha + \lambda_\alpha/\omega^2_\alpha)$. An entirely analogous treatment of $G_{\gamma\gamma'}$ shows that

$$G_{\gamma\gamma'} = G^0_{\gamma\gamma'} + V^i_{\gamma\gamma'} \quad , \tag{17}$$

with $V^i_{\gamma\gamma'} \simeq V^i(\vec{s}^{\,\gamma\gamma'})$ and $\vec{s}^{\,\gamma\gamma'}$ the minimum of V on the hypersurface $\gamma\gamma'$. We note that the V^is enter as additional potentials rather than as free-energy contributions.

From Eqs. (11), (16), and (17), we now find the mean jump rate

$$\langle w\rangle = (\eta N)^{-1}\sum_{\gamma}{}'\sum_{\gamma'}{}' P_\gamma \nu_{\gamma\gamma'} \times \exp\left(\frac{-\hat{g}_{\gamma\gamma'}}{k_B T}\right) \times \exp\left(-\frac{V^i_{\gamma\gamma'} - V^i_\gamma}{k_B T}\right), \quad (18)$$

with $\hat{g}_{\gamma\gamma'} = G^0_{\gamma\gamma'} - G^0_\gamma$ the activation energy in the virtual-crystal approximation and P_γ the configurational probability given by Eq. (10). Equation (18) is still general, and its use for solid electrolytes is only one specific application. In the alternative case of crystals supporting thermally activated disorder, for example, P_γ determines the most probable crystal configuration and the quantity of activated defect structure. The result therefore offers a theoretical description of materials such as AgCl and AgBr that contain strongly interacting assemblies of thermally activated defects. In the present work we fix attention on the alternative case of stronger disorder in which thermal activation determines only the relative occurrence of alternative defect arrangements rather than the density of the defects themselves.

We now make use of the translation symmetry of the virtual crystal to simplify Eq. (18). Suppose that distinguishable sites in the unit cell are labeled by $n = 1, 2, \ldots$ and the different jumps of the mobile unit from site n are identified using an additional index m. $\hat{g}_{nm}$ is now a constant for all jumps with a given (n,m). In addition, $\nu_{\gamma\gamma'}$ is sensitive mainly to local geometry and can be taken to depend principally on n and m; we therefore replace $\nu_{\gamma\gamma'}$ by ν_{nm} where appropriate. The sum over γ now defines an expectation value over n and that over γ' gives a factor ν_{nm} times the expectation value over jumps. Here ν_{nm} is the total number of jumps from n sites by m paths that are accessible in an average configuration of the mobile subsystem. With these substitutions, Eq. (18) becomes

$$\langle w\rangle = (\eta N)^{-1}\sum_{n}{}'\sum_{m}{}' \nu_{nm}\nu_{nm} \times \exp\left(\frac{-\hat{g}_{nm}}{k_B T}\right) \times \left\langle \exp\left(-\frac{V^i_{nm} - V^k_n}{k_B T}\right)\right\rangle. \quad (19)$$

Provided that we ignore minor temperature dependences of the ν_{nm} arising from changing short-range order, the entire many-body problem is reduced to the calculation of the expectation values in the last factor of Eq. (19).

To make first-principles predictions of the conductivity we need detailed knowledge of $V(\vec{s})$ in order to determine the quantities g_{nm}, V^i_{nm}, and V^i in Eq. (19). These details are not available at the present time. Equation (19) can nevertheless by used to interrelate conductivity and thermal properties. As a considerable oversimplification we model the relevant lattices as made only of equivalent sites and jump paths. The parameters therefore lose their dependence on n and m to leave

$$\langle w\rangle = (\eta N)^{-1}\nu\nu \exp\left(\frac{-\hat{g}}{k_B T}\right) \times \left\langle \exp\left(-\frac{\hat{V}^i - V^i}{k_B T}\right)\right\rangle \simeq (\eta N)^{-1}\nu\nu \exp\left(-\frac{\hat{g} + \langle V^i\rangle - \langle \hat{V}^i\rangle}{k_B T}\right), \quad (20)$$

in which V^i and $\hat{V}^i$ are written for the interaction potentials in the ground and saddle-point configurations.

In the introductory comments to this section it is established that the correlation factor for diffusion and the electrostatic drag in conduction are both order and temperature insensitive. When the diffusion coefficient D is first derived from $\langle w\rangle$, and the conductivity σ from D, using the Nernst-Einstein relationship, the preexponential is therefore found to be insensitive to temperature and local order [in fact, contributions of $T^{1/2}$ from ν and $\exp(-\hat{g}/k_B T)$ cancel T^{-1} from the Nernst-Einstein result]. To the extent that the remaining enthalpic portion of the virtual crystal $\hat{g}$ is temperature independent, one obtains the result

$$\frac{d(\ln\sigma)}{dT} = \frac{d}{dT}\frac{\langle V^i\rangle - \langle \hat{V}^i\rangle}{k_B T}. \quad (21)$$

All singular parts of the conductivity variation arise in this way from the interaction potential V^i.

We expect that the influence of local order on the saddle-point properties is rather weak. The point is that an accessible jump normally takes the migrating defect from its initially occupied site to one that is initially *un*occupied. The midpoint of the jump therefore samples the local order surrounding both an unoccupied site and an occupied site. In systems with approximately half the accessible sites occupied, the short-range orderings around filled and empty sites are complementary (they sum to uniformity when superposed). Whereas the initial state of the jump samples only the order around an occupied site, the saddlepoint samples equally the opposite ordering characteristics of full and empty sites, and is effectively decoupled from the order. In contrast, the initial configuration is strongly dependent on the order. To determine $V^i - \hat{V}^i$ we extract the active ion and replace it at its saddlepoint. In a pair-force model the mean energy needed to remove the mobile ion is just twice the experimentally accessible enthalpy h of interaction per particle. The energy to replace the ion at the saddle point is not known, but is probably small

and insensitive to order as mentioned above. We write $\langle \hat{V}^i \rangle = 2\mu h$ in the expectation that μ will be small and temperature insensitive. Then

$$\langle V^i \rangle - \langle \hat{V}^i \rangle = 2h(1-\mu) \quad . \tag{22}$$

From Eq. (22) we now obtain the singular part of the conductivity near the ordering temperatures T_c in the form

$$\frac{d(\ln\sigma)}{dT} \simeq \frac{2c_p(1-\mu)}{k_B T_c} + B \quad , \tag{23}$$

in which B contains all nonsingular contributions and $c_p = \partial h/\partial T$ is the specific heat due to interactions in the mobile-defect subsystem. Equation (23) is the final result we use to interpret the experimental data.

V. DISCUSSION

The results presented above establish that the $M\mathrm{Ag_4I_5}$ ionic conductors have very similar properties. Each exhibits an Ising-like order-disorder transformation near 200 K, around which the conductivity changes smoothly, but with a marked inflection. Our principal experimental results concern the specific heat and the ionic conductivity σ. In all three cases, we have determined the critical heat capacity ΔC_p and have found that σ conforms accurately to Eq. (4). It is the purpose of this discussion to use this experimental information to obtain further insight into the type of ordering that occurs and the way the order modifies the mobility.

We can use the specific-heat results to estimate the number of ions that order per formula unit. Suppose that at high temperature the 16 mobile ions per cell occupy the 56 available sites in a completely random manner. The configurational entropy per formula unit is then

$$S_{\mathrm{HT}} = 4R \ln\left(\tfrac{56}{16}\right) \tag{24}$$

at high temperature. To calculate the entropy at low temperature we assume that a fraction p of the 16 interstitials order and that each eliminates q sites from possible occupancy by other interstitials. The configurational entropy per formula unit of the remaining $16(1-p)$ mobile ions occupying $56-16\,pq$ sites is then

$$S_{\mathrm{LT}} = 4(1-p)R \ln[(56-16\,pq)/16(1-p)] \quad . \tag{25}$$

For the total entropy change due to the disordering transition we thus find

$$\Delta S = S_{\mathrm{HT}} - S_{\mathrm{LT}}$$

$$= 4pR \ln 3.5 - 4(1-p)R \ln\left(\frac{1-2pq/7}{1-p}\right) \quad . \tag{26}$$

This is the result needed to interpret the specific-heat data.

We can estimate the entropies of transition from the observed critical exponents and the amplitude of the observed critical heat capacity close to T_c. The results are as follows: $\Delta S = 4.0R$ ($\mathrm{RbAg_4I_5}$); $\Delta S = 3.4R$ ($\mathrm{KAg_4I_5}$); $\Delta S = 3.7R$ ($\mathrm{NH_4Ag_4I_5}$). Our value for the Rb salt agrees well with an earlier result.[4] We estimate the uncertainty in calculating the entropy changes at $\pm 10\%$ and therefore assume in the following $\Delta S = 3.7 \pm 0.3R$ for all three materials.

From Geller's x-ray study we note that the occupancies of many sites change dramatically below T_c. The occupancies of 14 sites are more than doubled, while 24 become vacant. The sites of increasing content contain 8.2 ions at the temperature of the measurement, indicating that $p \cong 8.2/16 = 0.51$. Since a total of 38 sites are involved, we conclude that $q = 38/16p \cong 4.6$. With these values we obtain $\Delta S = 3.4R$. This agrees with the experimental value from the specific-heat measurements within the experimental uncertainties. Further evidence for consistency between the thermal and diffraction data can be obtained from Eq. (26). When the observed values of ΔS are introduced into Eq. (26), one finds directly, for a wide range of possible values of p, that the value of pq lies in the range 40 ± 5. Thus, both the x-ray and specific-heat results indicate that approximately 40 of the 56 sites are excluded from occupancy in the fully ordered phase.

Consider now the mobility and its dependence on local order. We have seen that the experimental observations are accurately fitted by

$$\frac{d(\ln\sigma)}{dT} = \frac{\kappa \Delta C_p}{RT_c} \quad , \tag{4'}$$

both above and below the ordering temperatue and even in the "rounded" region at T_c. The experimental values of κ are collected in Table III. From the theory presented in Sec. IV we also have the result

$$\frac{d(\ln\sigma)}{dT} = \frac{2(1-\mu)c_p}{k_B T} \quad , \tag{23'}$$

with c_p the specific heat of interaction per mobile ion. It is highly satisfactory that the theory reproduces exactly the observed functional relationship between σ and the specific heat ΔC_p of ordering. We point out that the relationship (23) is independent of the specific ordering process and is equally valid in the absence of an order-disorder transformation. The transformation merely allows the interaction specific heat c_p to be separated from larger lattice contributions and thereby provides a definitive experimental verification of Eq. (23).

We conclude that the critical behavior of the mobility is one aspect of a much broader relationship between diffusion and interactions in dense assemblies

of defects. It is the short range order, included accurately in Eq. (23), that causes the mobility to exhibit explicit critical behavior not present in mean-field calculations. Our measurements are the first that possess the precision needed to compare the conductivity derivative with the heat capacity of disorder. No previous theories have succeeded in the incorporation of short-range order into accurate predictions. Sato and Kikuchi[22] have treated the short-range nature of the diffusion process in detail by a path probability method, but have made mean-field approximations to the thermodynamics. Lattice-gas models have been used[17] to incorporate short-range order but the transport properties have not been pursued to obtain accurate dc conductivities. In addition, it is necessary to treat the dynamics of hopping accurately to obtain Eq. (23), as noted in Sec. IV. We note that interesting diffusion anomalies of a related nature have been observed near the order-disorder transformations of hydrides,[23] but the interpretations were again tied to long-range, rather than short-range, order.

A comparison between Eqs. (4) and (23) offers further detailed information about the diffusion process. In an earlier brief report we point out that the experimental κ in Eq. (4) determines μ in Eq. (23), through the equation

$$\kappa \Delta C_p = 2N_A(1-\mu)c_p \ , \tag{27}$$

where N_A is Avogadro's number. The results of this comparison depend on the number of ions that contribute to the mobility. If all Ag ions per formula unit took part equally in the diffusion, ΔC_p would be apportioned equally among four ions so that $4N_A c_p = \Delta C_p$ and $4\kappa = 2(1-\mu)$. Using the observed κ one now finds $\mu_{Rb} = -0.22$ for $RbAg_4I_5$. The values for the other salts are: $\mu_{NH_4} = -0.36$ ($NH_4Ag_4I_5$); $\mu_K = -0.76$ (KAg_4I_5).

Equation (23) contains simplifying assumptions that are worth detailed mention here. If the available jump paths are not identical by symmetry, they can enter Eq. (19) with differing activation energies $\hat{g}$. Their contributions to σ are then weighted such that jumps with small $\hat{g}$ enhance the enthalpy contribution from their initial site in Eq. (23). A similar bias occurs for topological reasons if some sites take part in more than an average number of steps in the random walk each mobile ion travels. In the MAg_4I_5 lattices the type-II sites necessarily participate in all jumps and these are also the sites that order. For this reason the *effective* enthalpy per ion contributing to the mobility might be expected to exceed the average over all ions. A limiting estimate is obtained by assuming that only type-II sites contribute to the mobility. Approximately nine ions occupy type-II sites in both phases so that $2.25\kappa = 2(1-\mu)$. In this case $\mu_{Rb} = 0.32$, $\mu_{NH_4} = 0.24$, $\mu_K = 0.005$. The important point established by these numbers is that μ is small. In the two limiting cases of (a) all sites and (b) type-II sites alone contributing to the mobility, the deduced values of μ remain small and change sign between the extremes. We cannot treat the actual mobility processes in detail, but they must certainly lie between these two extremes. We conclude that μ is very close to zero in the real crystals. This confirms the intuitive belief, stated in Sec. IV, that the saddle points are decoupled from the local order. The reason is that each accessible saddle point samples equally the short-range order of the initially occupied site from which the mobile ion jumps and the short-range order of the initially *un*occupied final site.

A simple insight into the entire mobility process is now available. Neglecting all other free-energy contributions, in accordance with the linear-coupling approximation in Sec. IV, we regard the activation energy as a potential energy difference between a well bottom and a potential-barrier top. As the disordering progresses, the well bottom is lifted in proportion to the average interaction enthalpy h. The barrier height changes by $-2h(1-\mu)$ where the factor 2 accounts for the pairwise nature of the interaction potential and the factor $(1-\mu)$ takes account of (almost negligible) changes caused by the effect of order on the saddle point. The activation energy is then $-2h(1-\mu)+\text{const}$, and Eq. (23) follows immediately. The mobility thus reflects directly the way the well bottoms rise towards the saddle points as disordering progresses. Since none of the arguments involved in the theory are restricted to particular pressures, we expect both the precise treatment and this intuitive description of its consequences to hold for $h(T,p)$ acknowledged as a pressure dependent enthalpy.

We note finally that Eq. (4) holds with accuracy through the "rounded" region of the phase transition. We deduce from this that the inhomogeneities responsible for the rounding do not modify the topology of current flow significantly, or the relationship between heat capacity and conductivity would fail. One possible source of rounding is a local variation in T_c due to strains, low-angle boundaries, or fluctuations in impurity density. The variation ~ 0.1 K in T_c required by the observed rounding only involves a change $\sim 2\%$ in conductivity, since the peak observed value of $d(\ln\sigma)/dT$ is $\sim 0.15\ \text{K}^{-1}$.

Since changes in current path depend on the variations in the conductivity, their effect on the measured conductivity is of second order and therefore negligible. The observed changes in σ are evidently dominated by the first-order effects associated with the changes in *average* conductivity. Like the heat capacity, they are averages for the entire crystal, and the two properties therefore show identical rounding at T_c.

APPENDIX

The calculation of Sec. IV focuses on the effect of defect-defect interactions on the total jump rate. This

effect is of first order in the ordering energy and hence of second order in the ion-ion potential by which the mobile defects interact. It arises solely from the way the interactions change the diffusion barrier, and contains no description of the way inhomogeneities of the lattice from one site to the next influence the conductivity.

There is also a process of second order in the ion-lattice interaction potential that can cause large changes in the conductivity. It is a hydrodynamic effect that depends explicitly on *inhomogeneities* in the potential to which the mobile ions are exposed. Interactions among the mobile ions enter only through their effect on the dielectric function of the mobile assembly. Since interaction-induced short-range ordering modifies the response only to higher order in the ion-ion interaction, we can neglect defect ordering effects in a discussion of this second process.

Onsager's theory of the drag effect[24] in strong electrolytes is one example of the conductivity reduction caused by inhomogeneity. The inhomogeneity in that case arises from interactions between two defect systems having opposite charges. One may use Onsager's theory to estimate the drag caused by the anionic lattice on the mobility of Ag ions in solid electrolytes also, but the results are not reliable because the ionic density is too large. In addition, the crystal symmetry and the overlapping of nearby Debye-Hückel screening clouds introduces new effects that have not been described. This Appendix analyzes the effects of inhomogeneity on conductivity for a simple lattice model that suffices to illustrate in a qualitative way the basic processes that take place in solid electrolytes.

We fix attention on a model lattice in which the sites available to the mobile ions outnumber the ions by a factor 4. This is close to the ratio 7/2 that occurs in $M\mathrm{Ag}_4\mathrm{I}_5$. We will further suppose that the accessible sites for the mobile ions form a Bravais lattice. A simple cubic lattice with the anions occupying alternate cube centers in a bcc array provides an example that satisfied these conditions, and leaves all sites equivalent as desired.

The eigenfunctions of the diffusion equation on the Bravais lattice are plane waves with eigenvalues k that fill the Brillouin zone uniformly with density $(2\pi)^{-3}$.[25] Inhomogeneities described by these Fourier components of ion density decay with time constants τ_k that depend on the ion-ion interaction potential $\phi(r)$, through its Fourier transform ϕ_k. The relevant results are[25]

$$\tau_k^{-1} = \epsilon_k k^2 D, \quad \epsilon_k = 1 + C\phi_k/k_B T \ , \tag{A1}$$

with D the ionic diffusion coefficient and C the mean concentration of mobile ions. The dielectric function ϵ_k is the ratio of the applied to total potential Fourier component k at equilibrium. For the Coulomb interaction of concern here,[25]

$$\epsilon_k = (k^2+\kappa^2)/k^2 \ , \tag{A2}$$

with

$$\kappa^2 = 4\pi e^2 C/\epsilon k_B T \tag{A3}$$

the (squared) Debye-Hückel screening parameter and ϵ the lattice dielectric constant in the absence of defect mobility.

Suppose now that each anion exerts an interaction potential (energy) $\phi^0(r)$ on each mobile ion. It is shown elsewhere[20] that the interaction field from the mobile ions is changed by

$$\delta V(r) = -(2\pi)^{-3}\int_{\mathrm{BZ}} i\vec{k}\cdot\vec{v}\,\tau_k\phi_k^0 C_{k0} e^{i\vec{k}\cdot\vec{r}}\, d\vec{k} \ , \tag{A4}$$

when the mobile defects drift with velocity $\vec{v}$ past this anion. Here, C_{k0} is the Fourier coefficient of ion density at wave vector $\vec{k}$ in the equilibrium state of the system, and $\vec{r}$ is the distance from the anion to the test point. We now use the linearity of the defect-dielectric response to sum over all anions i, positions $\vec{R}_i$, to find the total interaction field

$$V(\vec{r}) = -(2\pi)^{-3}\int_{\mathrm{BZ}} i\vec{k}\cdot\vec{v}\,\tau_k\phi_k^0 C_{k0} \times \sum_i e^{i\vec{k}\cdot(\vec{r}+\vec{R}_i)}\, d\vec{k} \tag{A5}$$

or

$$V(\vec{r}) = -i(2\pi)^{-3}\sum_{\lambda=1}^{n}\vec{k}_\lambda\cdot\vec{v}\,\tau_\lambda\phi_\lambda^0 C_{\lambda 0} \times e^{i\vec{k}_\lambda\cdot\vec{r}}\sum_{j=1}^{n} e^{i\vec{k}_\lambda\cdot\vec{l}_j} \ . \tag{A6}$$

To obtain Eq. (A6) we have evaluated the summation over $\vec{R}_i$ to obtain δ functions at the lattice points k_λ of the anion reciprocal lattice. The basis distances $\vec{l}_j$ locate the n anions in the unit cell of the anion lattice. The mean force exerted by the mobile defects on the anion at $r=0$, and hence by symmetry the mean force exerted by the anions on each mobile ion, is obtained from Eq. (A6) as $[\vec{\nabla}V(\vec{r})]_{\vec{r}=0}$.

In the present application, the prescription (A6) has a trivial result. Because all sites are equivalent, the Fourier coefficients $C_{\lambda 0}$ of mobile ion density in equilibrium are all zero, other than that for $k_\lambda = 0$, for which $\vec{\nabla}V \equiv 0$. Consequently there is no drag whatever exerted on the mobile ions from the embedding lattice. In contrast, the Onsager result[24] for the effective mobility

$$\mu_{\mathrm{eff}} = \mu_0\left(1 + \frac{e^2\kappa}{3(2+\sqrt{2})Ck_BT}\right)^{-1} \tag{A7}$$

predicts incorrectly that the mobility μ_0 is reduced by more than an order of magnitude by the drag effect.

Our derivation shows explicitly how drag is associated with inhomogeneity of the equilibrating defect system, and how this inhomogeneity can be reduced to zero at high ion densities, thereby eliminating all drag.

The MAg_4I_5 lattices do not possess the exact equivalence of all anion sites assumed in the model system analyzed above. Consequently all Fourier coefficients $C_{\lambda 0}$ do not vanish and some drag effect is restored. A discussion of these corrections will not be presented here. For the present purposes it suffices to note that the relevant wave vectors $\vec{k}_\lambda$ required to give neighboring defect sites differing occupancies necessarily fall near the zone boundary where screening effects are minimal [cf. Eq. (A2)]. Interactions among the mobile defects play a much reduced role in the dynamical response for this regime. Furthermore, the observed concentration inhomogeneities over the three types of Ag site present in the MAg_4I_5 lattice are small compared to the very large effects predicted for Debye-Hückel screening at the near-neighbor distance in these concentrated defect systems. The drag is therefore much smaller than that predicted by Eq. (A7). Finally, the drag is temperature insensitive and cannot show significant critical behavior. Apart from the ordering that occurs on type-II sites of the lattice, the Ag concentrations at different sites in MAg_4I_5 are rather temperature independent. The ordering itself must be driven by defect interactions since, from symmetry, the virtual crystal potentials at the two type-II sites per cell are identical. Consequently the virtual crystal $C_{\lambda 0}$ for use in Eq. (A6) do *not* strongly reflect the critical behavior of the type-II site occupancies. Equation (A6) therefore remains temperature and order insensitive in the critical region, and the drag effect may be neglected from the discussion of Sec. IV, as mentioned there.

---

*Supported in part by NSF Grant No. NSF DMR-76-01058.

[1]*Fast Ion Transport in Solids: Solid State Batteries and Devices,* edited by W. van Gool (North-Holland, Amsterdam, 1973); *Superionic Conductors,* edited by G. D. Mahan and W. L. Roth (Plenum, New York, 1976).

[2]M. J. Rice and W. L. Roth, J. Solid State Chem. 4, 60 (1972).

[3]W. J. Pardee and G. D. Mahan, J. Solid State Chem. 15, 310 (1975).

[4]H. Wiedersich and W. V. Johnston, J. Phys. Chem. Solids 30, 475 (1969).

[5]F. L. Lederman, M. B. Salamon, and H. Peisl, Solid State Commun. 19, 147 (1976).

[6]S. Geller, Science 157, 310 (1967); Phys. Rev. B 14, 4345 (1976).

[7]M. B. Salamon, Phys. Rev. B 15, 2236 (1977).

[8]R. Vargas, M. B. Salamon, and C. P. Flynn, Phys. Rev. Lett. 37, 1550 (1976).

[9]L. A. Girifalco, *Statistical Physics of Materials* (Wiley, New York, 1973).

[10]Y. A. Kraftmakher, Zh. Prikl. Mekhan. Tekhn. Fiz. 5, 176 (1962); P. R. Garnier, Ph.D. thesis (University of Illinois, 1972) (unpublished).

[11]D. S. Simons, Phys. Rev. Lett. 26, 750 (1971); Ph.D thesis (University of Illinois, 1973) (unpublished).

[12]M. R. Manning, C. J. Venuto, and D. P. Boden, J. Electrochem. Soc. 118, 2031 (1971).

[13]B. B. Owens and G. R. Argue, Science 157, 308 (1967).

[14]R. A. vargas, Ph.D. thesis (University of Illinois, 1977) (unpublished).

[15]F. L. Lederman, M. B. Salamon, and L. W. Shacklette, Phys. Rev. B 9, 2981 (1974).

[16]Unfortunately there is no comprehensive review in this area, but the Arrhenius behavior of conductivity above the 200-K transition in the present materials provide one of many available examples.

[17]G. D. Mahan, Phys. Rev. B 14, 780, (1976).

[18]N. B. Slater, *Theory of Unimolecular Reactions* (Methuen, London, 1959).

[19]G. H. Vineyard, J. Phys. Chem. Solids 3, 121 (1957).

[20]For an introductory discussion, see C. P. Flynn, *Point Defects and Diffusion* (Oxford U.P., Oxford, 1972).

[21]These effects are discussed by Y. Adda and J. Philibert, *La Diffusion dans les Solides* (Universitaries de France, Paris, 1966).

[22]H. Sato and R. Kikuchi, J. Chem. Phys. 55, 677 (1971).

[23]Y. Fukai and S. Kazama, Acta Met. 25, 59 (1977).

[24]For a comprehensive review, see H. Falkenhagen, *Electrolytes* (Oxford U.P., Oxford, 1934).

[25]See the text in Ref. 20.